DOI: 10.61782/fa.2025.0225

FORUM ACUSTICUM EURONOISE 2025

COMPARATIVE DRONE NOISE FLIGHT TEST CAMPAIGN USING CONVENTIONAL PRECISION MICROPHONES AND AN ARTIFICIAL HEAD

Giovanni Fasulo[1*] **Francesco Petrosino**[1] **Mattia Barbarino**[1] **Luigi Federico**[1]

[1] Italian Aerospace Research Centre (CIRA), Capua (CE), 81043, Italy

ABSTRACT

This study investigates the acoustic signatures of a DJI Matrice 300 RTK during LiDAR and photogrammetric mapping missions at the Pianabella UrbanV vertiport in Rome. Utilizing a comprehensive setup that combines conventional precision condenser microphones with an artificial head, measurements were conducted throughout various drone flight phases. Analysis revealed that calculating advanced psychoacoustic metrics with the artificial head can introduce significant errors compared to conventional microphone measurements, for which these metrics were originally designed.

Keywords: *artificial head, psychoacoustic, drone noise, experimental test.*

1. INTRODUCTION

Small drones, known as Small Unmanned Aircraft Systems (sUAS), have become much more common in recent years, being used for commercial, security, and other purposes in areas that were previously unaffected [1]. As sUAS noise differs significantly from that of conventional aircraft [2], predicting resultant annoyance remains challenging. The numerous noise-generating components of sUAS experience constant variations in level, directionality, spectral content, and temporal characteristics during take-off, landing, and overflight maneuvers [3]. Moreover, the propagation of sUAS noise is highly sensitive to operating environment, weather, and wind conditions, complicating attempts to reliably forecast acoustic impacts. To address this, specialized flight tests are now crucial for better understanding sUAS noise and improving prediction models [4]. Within the European U-ELCOME project [5] framework, an extensive test campaign was carried out to investigate the acoustic signatures of different drone operations in real-world scenarios. Observations included different flight phases, such as take-off, overflight, and landing, to better characterize the role of operational aspects and external conditions on noise. A suite of precision microphones and an artificial head were deployed to capture a comprehensive dataset of both conventional and binaural acoustic measurements, which more accurately reproduce the subjective perception of human listeners. Traditional descriptors such as sound pressure level (SPL), along with psychoacoustic metrics including loudness, sharpness, fluctuation strength, roughness, and tonality, were computed for each audio sample. A comparative analysis between conventional microphone recordings and those acquired using an artificial head (both with and without the application of equalization curves) revealed significant discrepancies. These findings underscore the importance of a careful and informed application of psychoacoustic measurement equipment and metrics when assessing the potential disturbance caused by sUAS noise. Moreover, the results highlight the critical role of flight test data in developing robust acoustic impact evaluation methods, which are essential for guiding future regulatory frameworks and design considerations.

**Corresponding author*: G.Fasulo@cira.it.

Copyright: ©2025 First author et al. This is an open-access article distributed under the terms of the Creative Commons Attribution 3.0 Unported License, which permits unrestricted use, distribution, and reproduction in any medium, provided the original author and source are credited.

2. TEST GROUND AND EQUIPMENT

2.1 Test Ground

The acoustic test campaign was conducted on November 28th 2024 at the Pianabella UrbanV vertiport in Rome, Italy, with the primary objective of capturing and analyzing noise emissions during LiDAR and photogrammetric terrain mapping operations. The experimental setup involved the deployment of precision condenser microphones across the test field (Figure 1) to accurately record the acoustic signatures associated with various drone activities: takeoffs, landings, and flyovers. This approach enabled a comprehensive assessment of the drone's noise profile under realistic operational conditions.

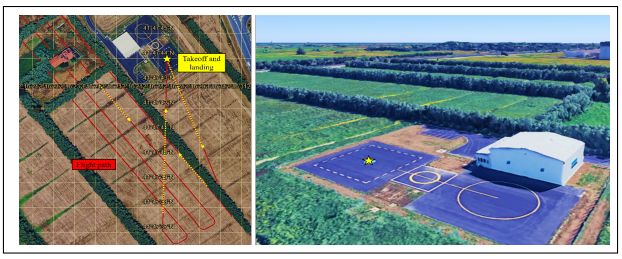

Figure 1. Test ground and planned drone flight path (Google Earth image).

2.2 Acoustic Equipment

Acoustic measurements were conducted using a comprehensive system that integrates data acquisition hardware, precision microphones, signal conditioning components, and calibration tools. The setup comprised a personal computer interfaced with an IMC C-SERIES PL3 analyzer, which provided eight channels at a sampling rate of 50 kHz per channel. Acoustic signal acquisition was achieved using a set of precision pre-polarized condenser microphones coupled with dedicated preamplifiers. Specifically, eight PCB model 377B11 microphones, which feature a pressure-field response were deployed. Each microphone has a nominal 1/2-inch diameter and a typical sensitivity of 50 mV/Pa, with the 377B11 units covering a frequency range of 3.15 to 10000 Hz (±2 dB) and a dynamic range of 146 dB re 20 µPa. Prior to measurements, each microphone was calibrated using a PCB model CAL250 acoustic calibrator that provides a 250 Hz output at 114 dB re 20 µPa (±0.2 dB) with distortion below 2%. Windscreens were employed on each microphone to mitigate wind-induced noise from high-speed airflow. To preserve signal integrity over long cable runs and extend the measurable frequency range, 8 microphone preamplifiers (PCB model 426A30) equipped with 7-pin LEMO connectors were used. These preamplifiers, which produce an output voltage of 28 Vpp, were supplied by 8 preamplifier power supplies (Larson Davis model 2221). These supplies offer selectable polarization settings (0 and 200 V) and weighting options (A, C, or Z), with a frequency response (Z-weighted) from 10 Hz to 100 kHz (±0.2 dB) and 1 Hz to 150 kHz at –3 dB. In addition, CIRA deployed a specialized acquisition system known as an artificial head, which replicates the acoustically significant features of the human ear, head, shoulders, and skin. This design filters incoming sound based on its direction, enabling the recorded signals to be perceived as if the listener were immersed in the original sound field. The artificial head HSU III.2 incorporates two precision pre polarized condenser microphones that have a nominal diameter of 1/2 inch and a typical sensitivity of 50 mV/Pa. These microphones operate over a frequency range of 3.5 to 20000 Hz, offer a dynamic range of 119 dB re 20 µPa, and can handle sound pressure levels up to 135 dB with less than 3% distortion at 1 kHz. Data acquisition and storage were managed using SQobold, a four channel recording and playback system for mobile sound and vibration measurements, providing two channels with a sampling rate of 48 kHz per channel.

Figure 2 is a sketch of the experimental apparatus schematic diagram:

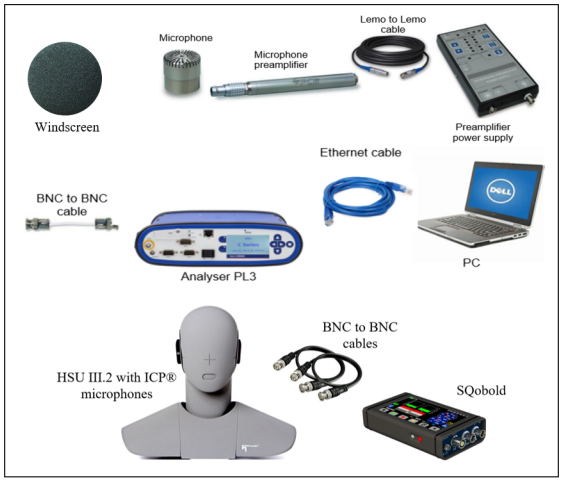

Figure 2. Experimental apparatus schematic diagram.

Microphone placements were determined based on the drone's designated flight paths (Figure 3). Three microphones were arranged in a quarter-circle with a 7-meter radius at a height of 1.5 meters, centered on the drone's takeoff point. A second array, consisting of three microphones, was configured in a quarter-circle with a 14-meter radius, also at 1.5 meters above ground level. In addition, two microphones were positioned along the drone's flight path within the terrain adjacent to the Pianabella vertiport, maintaining the same 1.5 meter elevation. Furthermore, the artificial head was mounted on a tripod and oriented such that its shoulders were perpendicular to the drone's flight trajectories, with the left ear directed toward the takeoff point, aligned with the position of microphone #8 (Ch8). The ear level was set at 1.5 meters from the ground.

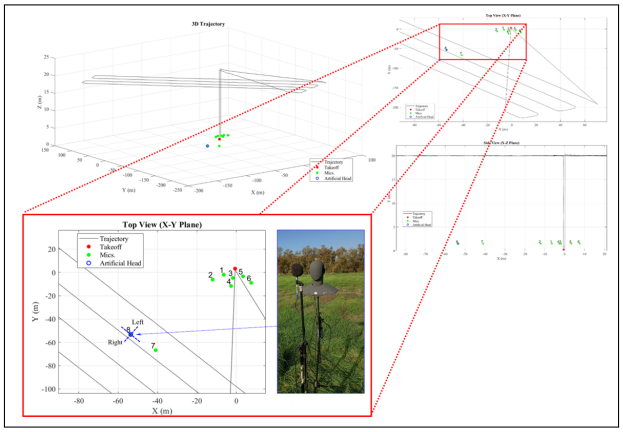

Figure 3. Drone trajectory and acoustic sensors locations.

2.3 Test Article

For the LiDAR and photogrammetric mapping operations, a DJI Matrice 300 RTK quad-rotor (Figure 4) was deployed. This versatile platform is engineered for a wide range of industrial applications and features a robust, foldable design that ensures both durability and ease of transport across various operational environments. Its support for multiple payload configurations allows for tailored setups to meet specific mission requirements, while advanced flight control algorithms and GPS positioning deliver precise navigation, stable hovering, and autonomous operation capabilities. The main technical specifications of the DJI Matrice 300 RTK are as follows: when unfolded (without propellers), its dimensions are 810 × 670 × 430 mm, and when folded (with propellers), 430 × 420 × 430 mm, with a diagonal wheelbase of 895 mm. The drone weighs approximately 3.6 kg without batteries and around 6.3 kg when equipped with batteries, with a maximum takeoff weight of 9 kg. It supports a maximum payload capacity of 2.7 kg and offers a flight time of up to 55 minutes with no payload.

Figure 4. DJI Matrice 300 RTK at UrbanV vertiport.

3. ACOUSTIC MEASUREMENTS AND POST-PROCESSING

This section presents the methodology employed for acoustic measurements at the UrbanV vertiport in Rome. Data acquired from both precision microphones and an artificial head were analyzed to assess the implications of the observed noise signatures.

3.1 Background Noise

Background noise plays a critical role in acoustic measurements as it represents the ambient sound environment in the absence of the primary noise source. In this study, the drone serves as the primary noise source, while the background noise is primarily attributable to operations at a nearby airport. This background noise includes sounds from aircraft takeoffs and landings, ground support equipment, vehicular traffic, and other related activities. Consequently, precise measurement of the background noise is imperative for establishing a reliable baseline that differentiates between ambient environmental noise and the noise generated specifically by the drone. To achieve this, acoustic signals were recorded and analyzed for approximately 150 seconds before to the beginning of the flight

test. The post-processing involved applying a Discrete Fourier Transform (DFT) with a Hanning window and a 50% overlap. Given the signal duration and segmentation, a sampling frequency of 0.01 Hz was achieved. Specifically, the signal was segmented into two overlapping frames, with each frame windowed by the Hanning function to minimize spectral leakage. The 50% overlap ensured that each consecutive frame shared half of its data points with the previous frame, thereby enhancing frequency resolution and yielding a smoother, more reliable frequency spectrum. The DFT was computed for each windowed segment, and the resulting spectra were averaged. To facilitate interpretation, the spectra were converted into 1/3 octave bands and adjusted using A-weighting (Figure 5) to account for the human ear's varying sensitivity across frequencies.

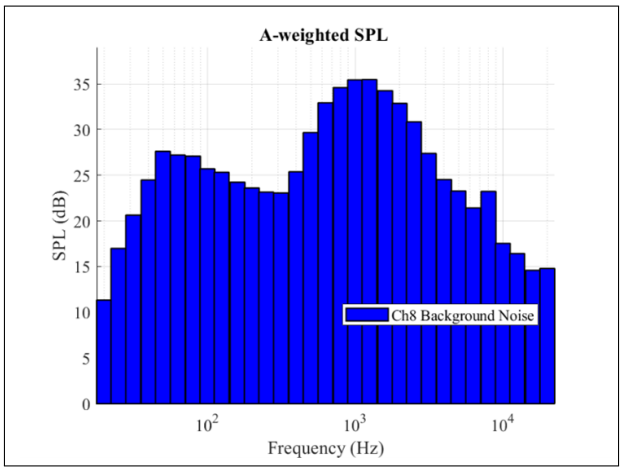

Figure 5. A-weighted 1/3 octave band spectra of background noise recorded by microphone #8.

Additionally, the mean A-weighted Overall Sound Pressure Level (A-OASPL) from all microphone measurements, which represents the mean total sound energy over the measurement duration, was computed. Specifically, two mean A-OASPL values were computed to reflect the distinct environmental conditions at different measurement locations. Microphones #1 to #6, positioned near the takeoff and landing area on rigid asphalt surfaces, exhibited a mean A-OASPL of 47.8 dBA, likely due to increased sound reflections. In contrast, microphones #7 and #8, deployed on grass and other absorptive surfaces, recorded a lower background noise level of 43.8 dBA, resulting from enhanced sound absorption.

3.2 Drone Noise

The acoustic signature of drones substantially differs from that of conventional aircraft. Drone noise is characterized by a complex frequency spectrum featuring multiple tones at harmonics of the blade passage frequency (BPF). Moreover, these acoustic emissions can vary considerably depending on factors such as drone type, size, propeller design, and operational conditions. Consequently, conventional noise metrics like $L_{A,eq}$ or L_{AE} are often inadequate to capture the annoyance of drone noise, thereby necessitating the use of psychoacoustic parameters that more accurately reflect human auditory perception.

Within the framework of the U-ELCOME project, a series of tests were conducted to characterize the noise generated by drones. The main test lasted 755 seconds, with signal acquisition for the eight microphones started and ended manually at the beginning and end of each test session. In contrast, the psychoacoustic head was activated manually prior to the initial test and deactivated after all tests, resulting in a continuous recording from which the relevant sections were later extracted. To analyze the temporal evolution of the drone's spectral content, a spectrogram was computed. This analysis utilized a Hanning window with a 50% overlap. The FFT was computed with a spectrum size of 65536 samples at a sampling rate of 50 kHz, resulting in time and frequency resolutions of 1.31 seconds and 0.76 Hz, respectively. Given the tonal nature of the recorded noise and the absence of impulsive characteristics, a larger FFT size was selected to achieve finer frequency resolution. Figure 6 presents the spectrograms for microphones #7 and #2.

These spectrograms reveal a predominance of continuous low-frequency noise attributable to background noise. In the recordings from microphone #2, peaks in the mid-to-high frequency range were observed at the beginning and end of the test, corresponding to the drone's noise during takeoff and landing. Conversely, recordings from microphone #7 exhibited peaks at regular intervals, characteristic of drone overflights. In the frequency domain, periodic spectral lines corresponding to the harmonics of BPF are clearly discernible. These harmonics are most marked when the drone is close to the microphones but become increasingly diluted by ambient noise as the drone moves farther away.

3.2.1 Artificial Head vs. Conventional Microphone

The artificial head employed in this study inherently incorporates multiple filtering phenomena, namely, pinna

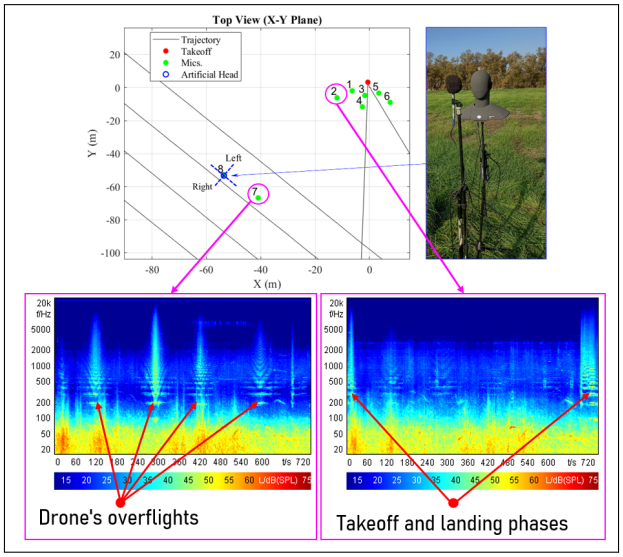

Figure 6. Drone path, placement of acoustic equipment, and corresponding spectrograms.

effects, ear canal resonance, diffraction and reflection due to the head's structure, acoustic shadowing, and skin absorption. These effects result in distortions that make the signals captured by the artificial head incompatible with those obtained from conventional measurement microphones [6]. Consequently, parameters such as the A-weighted sound pressure level and various other metrics cannot be reliably determined using a non-equalized artificial head measurement system. To address this limitation, HEAD Acoustics provides three distinct equalization options for the artificial head based on the direction of sound incidence:

- Free Field (FF): Sound arriving from the front in an anechoic environment, with the sound source located at least 3 meters from the artificial head;
- Diffuse Field (DF): Sound arriving uniformly from all directions;
- Independent of Direction (ID): Equalization tailored to the directional resonances of the cavum conchae and the ear canal entrance.

Since the sound field conditions during measurement rarely correspond exactly to any one of these idealized scenarios (FF, DF, or ID) this study examined the influence of various equalization curves on the evaluation of psychoacoustic metrics. For this purpose, microphone #8 was strategically positioned adjacent to the artificial head along the drone's flight path, specifically between the two ear microphones. A slight spatial displacement was compensated by temporally shifting the microphone pressure time histories by 0.45 seconds. Acoustic levels are presented in Figure 7 without the application of any weighting functions, ensuring an accurate representation of the total acoustic energy and to clarify the underlying noise generation mechanisms. Only a slow time weighting (1000 ms) was applied to smooth the output and enhance the readability of the plot.

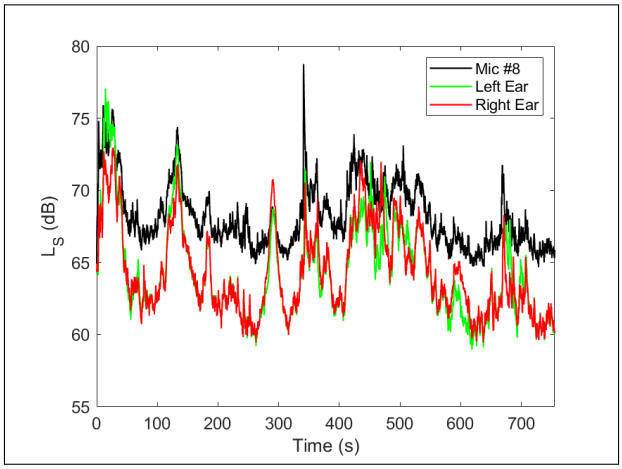

Figure 7. Acoustic levels with slow time weighting for conventional microphone #8 and the artificial head's ear microphones.

Microphone #8 generally records higher levels than the ear microphones, although there are time intervals where the levels converge or where the ear microphones briefly exceed those of microphone #8. Furthermore, the slight mismatch between left and right ear measurements arises from the head's asymmetry relative to the sound source. Refer to Figure 3 for an overview of the flight path and the artificial head's positioning.

The subsequent analysis focuses on a single forward flight segment, specifically, the time interval during which the drone is nearly overhead of the artificial head, as indicated between 200 and 370 seconds in the level graph (Figure 7). Figure 8 compares the spectral content of both recordings within the human auditory range (20 Hz–20 kHz). The spectra were computed using a Fast Fourier Transform (FFT) with a spectrum size of 16384 samples, a Hanning window, and 50% overlap. Given the 50 kHz

sampling frequency, the frequency resolution is approximately 3 Hz. These measurement do not incorporate any equalization curves, thereby representing the spectra of the original recorded sound.

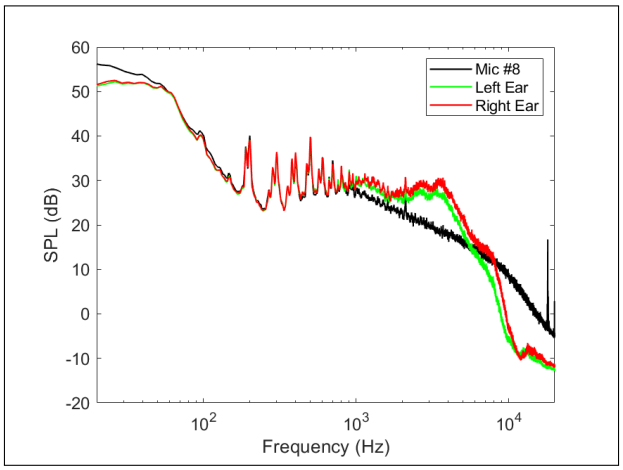

Figure 8. Comparison of the acoustic spectra obtained from conventional microphone #8 and the artificial head's ear microphones during the drone's forward flight.

The tonal components, specifically, the first eight harmonics of the blade passing frequency (BPF), are captured equally by both the conventional microphone and the artificial head. In the forward flight scenario, Figure 8 illustrates the separation of the BPFs between the forward and aft rotors, a result of the differing rotation rates during this flight condition. However, the artificial head also exhibits additional peaks at approximately 3 kHz, which indicate resonance associated with the ear canal's length [7], while a notch across the entire frequency band at 10 kHz can be attributed to the effect of the pinna [8]. The difference in the low-frequency region is likely due to the transition from free-field conditions to a duct configuration, which introduces a change in acoustic impedance that conventional microphones do not account for. This discontinuity may induce partial reflections of the acoustic wave at the entrance of the ear canal, thereby reducing the energy transmitted within the duct and consequently attenuating the signal detected by the artificial head microphones.

The following graphs present the FFT computed using equal input settings and time histories previously employed, incorporating the combined effect of the three equalization curves provided by HEAD Acoustics. In each instance, the resulting spectra are compared with those derived from conventional microphone recordings of the same noise event.

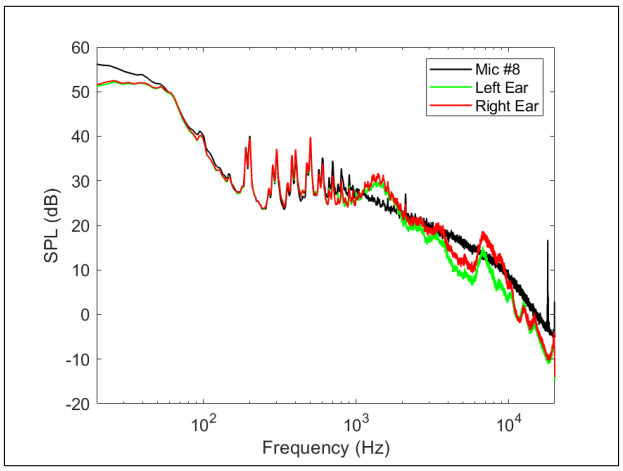

Figure 9. Conventional microphone #8 versus the artificial head's ear microphones (FF equalized).

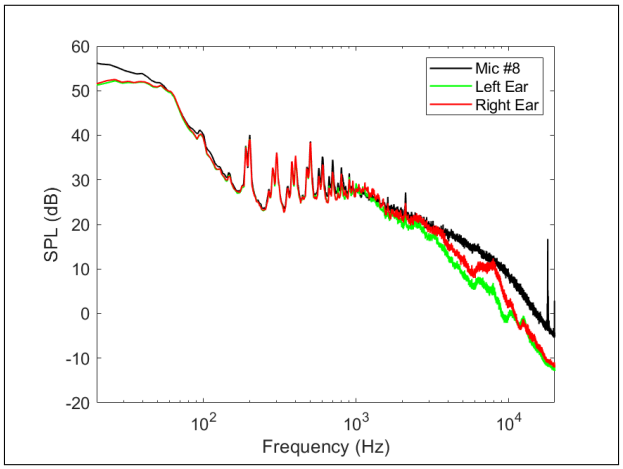

Figure 10. Conventional microphone #8 versus the artificial head's ear microphones (DF equalized).

Analysis reveals that the equalization curves do not reconstruct the spectral content of the conventional microphone signal from artificial head measurements with high fidelity. In this context, the diffuse field equalization appears to be a more suitable option. A quantitative evaluation of psychoacoustic metrics is provided in the subsequent part of this work. Specifically, Sound Quality (SQ)

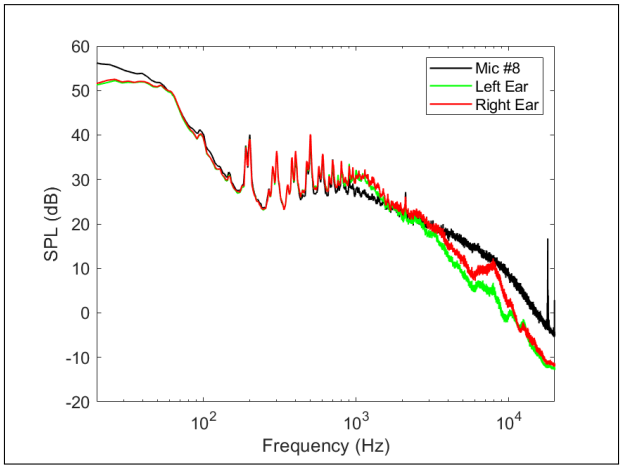

Figure 11. Conventional microphone #8 versus the artificial head's ear microphones (ID equalized).

metrics were computed for the conventional microphone recordings and for the artificial head measurements (both with and without equalization) across distinct phases of the drone mission. For this purpose, the levels shown in Figure 7 were segmented into six sub-signals with time ranges of 1–60, 60–200, 200–370, 370–530, 530–660, and 660–755 seconds. The analyses were conducted using the ArtemiS software from HEAD Acoustics, and the computed SQ metrics include Loudness (N), Roughness (R), Fluctuation Strength (F), Sharpness (S), and Tonality (T).

Loudness, Roughness, and Tonality were calculated according to ECMA-418-2 (2nd Edition), based on the Sottek Hearing Model [9]. In particular, for the computations of Loudness and Roughness, signals from both the right and left ears of the artificial head were combined. The calculation of Fluctuation Strength was derived from that of Roughness, with an adaptation ensuring that its maximum value occurs at a modulation frequency of 4 Hz. Finally, Sharpness was determined using the DIN 45692 standard. The maximum value, along with the 5th and 10th percentiles of each audio sample, was computed and analyzed. For metrics that lack an inherently defined combined left/right ear result (Fluctuation Strength, Sharpness, and Tonality) the arithmetic mean of the left and right ear values was employed as the representative single value metric for the artificial head. To ensure consistency, the mean absolute differences between the conventional and equalized curves, computed across all tests, were normalized by the mean metric value as estimated by the conventional microphone. Consequently, Figure 12 to Figures 15 illustrate the percentage deviation from the expected results for each single value metric and for each equalization curve adopted.

No eq. curve			
	Max	5%	10%
N	15.8	16.8	17.8
R	11.1	12.3	12.1
F	6.8	13.6	7.4
S	29.9	18.2	3.4
T	26.1	7.1	12.0

Figure 12. Percentage deviation from the expected results (Not Equalized).

FF			
	Max	5%	10%
N	2.8	3.6	3.4
R	13.9	16.3	17.9
F	3.7	7.6	4.3
S	31.9	22.2	2.9
T	8.2	9.6	9.6

Figure 13. Percentage deviation from the expected results (FF Equalized).

4. CONCLUSIONS

As part of the U-ELCOME project, an acoustic test campaign was conducted on November 28th 2024 at the Pianabella UrbanV vertiport in Rome, Italy. The study aimed to record and analyze the noise generated by a DJI Matrice 300 RTK during LiDAR and photogrammetric mapping operations. To achieve this, CIRA deployed eight 1/2-inch precision condenser microphones alongside an artificial head, strategically placing the sensors across the test field to capture noise during drone take-offs, landings, and overflights. A comparative analysis of psychoacoustic metrics derived from conventional microphone measurements and those obtained from the artificial head, both with and without equalization curve, revealed significant differences. Overall, the application of equalization curves substantially improves loudness estimation.

DF			
	Max	5%	10%
N	7.1	5.5	5.1
R	13.8	12.7	15.7
F	2.6	5.0	3.9
S	37.9	11.3	6.3
T	11.1	14.1	14.5

Figure 14. Percentage deviation from the expected results (DF Equalized).

ID			
	Max	5%	10%
N	3.3	4.2	3.9
R	16.0	19.5	24.5
F	3.2	8.5	4.3
S	39.1	7.5	9.1
T	11.1	14.6	17.8

Figure 15. Percentage deviation from the expected results (ID Equalized).

In particular, the "free-field" equalized curve yields the most accurate loudness estimates when compared with the reference measurement obtained from a conventional microphone. Other metrics did not exhibit a clear or consistent pattern. These results underscore that if the objective of using the head is to estimate psychoacoustic metrics in contexts that differ from the idealized conditions of a free-field or diffuse field, even when applying the "independent of direction" equalization curve as recommended by HEAD Acoustic for that cases, non-negligible errors may arise. Consequently, it may be valuable to develop specialized metrics for head measurements that eliminate the need for equalization by directly quantifying the external hearing effect during testing.

5. ACKNOWLEDGMENTS

The authors would like to thank all the partners of the U-ELCOME project, with special thanks to UrbanV for hosting the test campaign and to TopView for providing the drone.

6. REFERENCES

[1] B. Schäffer, R. Pieren, K. Heutschi, J. M. Wunderli, and S. Becker, "Drone noise emission characteristics and noise effects on humans—a systematic review," *International Journal of Environmental Research and Public Health*, vol. 18, no. 11, p. 5940, 2021.

[2] A. W. Christian and R. Cabell, "Initial investigation into the psychoacoustic properties of small unmanned aerial system noise," in *Proceedings of the 23rd AIAA/CEAS Aeroacoustics Conference*, p. 4051, 2017.

[3] A. J. Torija, Z. Li, and R. H. Self, "Effects of a hovering unmanned aerial vehicle on urban soundscapes perception," *Transportation Research Part D: Transport and Environment*, vol. 78, p. 102195, 2020.

[4] R. Cabell, F. Grosveld, and R. McSwain, "Measured noise from small unmanned aerial vehicles," in *Inter-Noise and Noise-Con Congress and Conference Proceedings*, vol. 252, pp. 345–354, Institute of Noise Control Engineering, June 2016.

[5] EUROCONTROL, "U-ELCOME." `https://www.eurocontrol.int/project/u-elcome`, January 25 2023. Accessed: [Insert access date here].

[6] H. acoustics GmbH, "Part 3: Equalization of binaural recording," in *Application Notes, SVP Series*, n.d. HEAD acoustics GmbH, 52134 Herzogenrath, Germany. Available at: `https://cdn.head-acoustics.com/fileadmin/data/global/Application-Notes/SVP/Part-3-Equalization_of_binaural_recording_e.pdf`.

[7] Sugiyama, Kiyoshi, Nishimoto, Mitsugu, and Satoh, Machiko, "Transmission characteristics of ear canal of artificial head," *Acoustical Science and Technology*, vol. 26, no. 1, pp. 67–70, 2005.

[8] Sugiyama, Kiyoshi, "Sound collection effect of a pinna of an artificial head," *Acoustical Science and Technology*, vol. 24, pp. 311–314, 2003.

[9] R. Sottek, "Application of the sottek hearing model for environmental noise assessment," in *Proceedings of the Institute of Acoustics, Vol. 46. Pt. 2*, 2024. HEAD acoustics GmbH, 52134 Herzogenrath, Germany.